HHS Public Access

Author manuscript

Adv Funct Mater. Author manuscript; available in PMC 2020 August 27.

Published in final edited form as:

Adv Funct Mater. 2017 July 19; 27(27): . doi:10.1002/adfm.201606614.

Elastomeric Fibrous Hybrid Scaffold Supports In Vitro and In Vivo Tissue Formation

Nafiseh Masoumi,
Department of Cardiac Surgery, Boston Children's Hospital, 300 Longwood Avenue, Boston, MA 02115, USA

Harvard-MIT Health Science and Technology, Department of Medicine David H. Koch Institute, 500 Main St. Cambridge, MA 02139, USA

Dane Copper,
Department of Cardiac Surgery, Boston Children's Hospital, 300 Longwood Avenue, Boston, MA 02115, USA

Peter Chen,
Department of Cardiac Surgery, Boston Children's Hospital, 300 Longwood Avenue, Boston, MA 02115, USA

Alexander Cubberley,
Department of Cardiac Surgery, Boston Children's Hospital, 300 Longwood Avenue, Boston, MA 02115, USA

Kai Guo,
Tepha, Inc., Lexington, MA 02421, USA

Ruei-Zeng Lin,
Department of Cardiac Surgery, Boston Children's Hospital, 300 Longwood Avenue, Boston, MA 02115, USA

Harvard Medical School, Longwood Avenue, Boston, MA 02115, USA

Bayoumi Ahmed,
Department of Cardiac Surgery, Boston Children's Hospital, 300 Longwood Avenue, Boston, MA 02115, USA

David Martin,
Tepha, Inc., Lexington, MA 02421, USA

Elena Aikawa,
Harvard Medical School, Longwood Avenue, Boston, MA 02115, USA

john.mayer@cardio.chboston.org.

Supporting Information
Supporting Information is available from the Wiley Online Library or from the author.

Conflict of Interest
The authors declare no conflict of interest.

Vascular Biology Program, Center for Interdisciplinary Sciences at Brigham and Women's Hospital, Boston, MA, USA

Juan Melero-Martin,
Department of Cardiac Surgery, Boston Children's Hospital, 300 Longwood Avenue, Boston, MA 02115, USA

Harvard Medical School, Longwood Avenue, Boston, MA 02115, USA

John Mayer
Department of Cardiac Surgery, Boston Children's Hospital, 300 Longwood Avenue, Boston, MA 02115, USA

Harvard Medical School, Longwood Avenue, Boston, MA 02115, USA

Abstract

Biomimetic materials with biomechanical properties resembling those of native tissues while providing an environment for cell growth and tissue formation, are vital for tissue engineering (TE). Mechanical anisotropy is an important property of native cardiovascular tissues and directly influences tissue function. This study reports fabrication of anisotropic cell-seeded constructs while retaining control over the construct's architecture and distribution of cells. Newly synthesized poly-4-hydroxybutyrate (P4HB) is fabricated with a dry spinning technique to create anelastomeric fibrous scaffold that allows control of fiber diameter, porosity, and rate ofdegradation. To allow cell and tissue ingrowth, hybrid scaffolds with mesenchymalstem cells (MSCs) encapsulated in a photocrosslinkable hydrogel were developed. Culturing the cellularized scaffolds in a cyclic stretch/flexure bioreactor resulted in tissue formation and confirmed the scaffold's performance under mechanical stimulation. In vivo experiments showed that the hybrid scaffold is capable of withstanding physiological pressures when implanted as a patch in the pulmonary artery. Aligned tissue formation occurred on the scaffold luminal surface without macroscopic thrombus formation. This combination of a novel, anisotropic fibrous scaffold and a tunable native-like hydrogel for cellular encapsulation promoted formation of 3D tissue and provides a biologically functional composite scaffold for soft-tissue engineering applications.

Keywords

bioreactors; fibrous scaffolds; hybrid scaffolds; photodegradable hydrogels; tissue engineering

1. Introduction

Synthesis and fabrication of naturally derived biomaterials or synthetic polymers to mimic the structural and mechanical characteristics of native tissues has been the focus of tissue engineering (TE) for more than a decade. Modern biomaterials, however, are not without limitations. One of the most challenging aspects of restoring and/or improving a native tissue's physiological function with engineered constructs is timing simultaneous transformation: the progression from synthetic to native structure. Though structural support for damaged tissue is essential,[1,2] mechanical integrity can impact the functionality of host tissue (i.e., both soft and hard tissue).[3] This is especially true for constructs that are not

cellularized before implantation. Without native tissue ingrowth onto the implanted scaffold, specifically within the context of cardiovascular applications, physiological conditioning can affect the durability of the scaffolds through repetitive flexion and extension cycles. This scaffold fatigue could be mitigated by introducing living cells into the scaffold's structure that are then capable of extracellular matrix (ECM) repair and remodeling.

When designing functional scaffolds, fundamental requirements must first be considered. The scaffold must: (1) imitate native mechanical (elasticity and deformation) and structural properties (ECM fiber alignment),[4–6] (2) facilitate cellular growth, tissue formation, and vasculari-zation,[1,7] and (3) possess controlled bio-degradability.[6,8] Previous attempts to design synthetic scaffolds from polymers have captured a number of these characteristics.[5,6,9–14] However, many of these materials have other notable shortcomings, including inelasticity (e.g., polyglycolic acid and polylactic acid, PGA and PLA, respectively),[11] plastic deformation and slow degradation over time (e.g., polycaprolactone (PCL)),[6] low porosity, and resulting poor cellular penetration (polyurethane (PU) sheets[13]), and a lack of fibrous structure (poly glycolic sebasic acid (PGS)[9,10]) or anisotropic characteristics (e.g., poly-carbonate-/ester-urethane urea) (PCUU/PEUU)[14] and poly(3-hydroxybutyrate-co-4-hydroxybutyrate) (P(3HB-co-4HB)).[13] In addition to synthetic material, natural hydrogels, including collagen and fibrin hydrogels, are notable for their ease of fabrication and their superior cellular retention[15] (due to the presence of natural protein, collagen fibers, and glycosaminoglycans (GAG)[16,17]), yet they lack mechanical integrity and have proven to be difficult to suture.

Using newer fabrication techniques, fibrous scaffolds have shown improved mechanical properties and fiber alignment providing anisotropy similar to native tissue.[6] Although, these techniques result in nano and microfibers, they have demonstrated reduced porosity and have inhibited cellular penetration into the construct, preventing 3D tissue formation.[8,12,18] Therefore, integrating cells within the 3D structure of scaffolds remains a primary challenge. Cellular encapsulation within hydrogels has shown preliminary success in generating a cel-lularized 3D construct.[19] The application of hydrogels for soft tissue regeneration has been reported extensively, particularly in the design and fabrication of cell laden materials for wound healing, implantable tissues, and tissue repair.[20] To control the hydrogel structure and mechanical properties, researchers have incorporated photodegradable moieties into the synthetic hydrogels. Our group recently demonstrated that methacrylated gelatin (GelMa) hydrogel provided promising results for generating tissues and vascular networks within the hydrogel, with properties that could be modulated and optimized on the basis of timing the photopolymerization and crosslinking of GelMa.[16,21] Similar to many naturally based hydrogels, throm-bogenicity, suboptimal mechanical properties, poor durability, and decreased cellular spreading, however, were limitations that also accompanied these acellular hydrogel materials.[22] similar to other hydrogel based materials used for scaffolding for tissue engineering.

Various native tissues comprise of dense ECM fibers as well as hydrogel like content. For example, native aortic and pulmonary valve leaflets are comprised of two dense ECM fibrous layers (of collagen and elastin proteins) and a hydrogel-like layer (containing glycosaminoglycan protein). In this study, we attempted to integrate the advantages of both

synthetic biocompatible polymers in the form of fibrous scaffolds (structure and mechanics) and hydrogels (cellular retention properties) to create a novel, hybrid scaffold applicable for various soft tissue engineering. We fabricated a microfibrous scaffold based on newly synthesized poly-4-hydroxybutyrate (P4HB),[23] with favorable biomechanical properties (i.e., elasticity and deformation in the physiological range, 15%−20% strain for native tissues), anisotropy, and more rapid degradation. We then addressed the issue of cellular ingrowth by integrating mesenchymal stem cells (MSCs) into the 3D fibrous structure of the scaffold using the photo-crosslinkable hydrogel, GelMa. The synergistic properties of P4HB and GelMa were combined to create a biomimetic hybrid scaffold (P4HB/GelMa) with desired biomechanics and a hospitable environment in which cells can grow and proliferate. Understanding the role of mechanical forces on cell behavior is critical for tissue engineering, so bioreactor systems have been designed to mimic the physiological and tissue-specific in vivo environment.[24,25] Following hybridization, we conditioned the cellularized scaffold in a stretch-flex bioreactor to further promote cell growth while evaluating the scaffold's endurance under mechanical stimulation. The combination of an anisotropic, fibrous scaffold, and a tunable, native-like hydrogel for cellular encapsulation enhanced the formation of 3D tissue and provided a biologically functional, hybrid scaffold for in vivo implantation.

2. Results and Discussion

2.1. P4HB Demonstrates Favorable Mechanics and Structural Anisotropy

Fiber alignment was created using a rotating mandrel as a collector during a dry spinning procedure at a speed of 1166 rpm (Figure 1A). Fibers were better oriented in the aligned scaffolds versus random scaffolds as shown in scanning electron microscope (SEM) images (Figure 1B,C). This resulted from the variations in the collector of the dry spinning procedure (rotating mandrel vs stationary flat collector). Random fibers were generated by dry spinning the raw material onto an immobile conductive surface, which pulled fibers in various directions. Aligned fibers were generated by spinning raw material onto a rotary mandrel rotating, perpendicular to the angle at which raw material was ejected from the source needle. Fiber alignment for both random and aligned fibers was quantified using ImageJ graphical analysis of SEM images (data not shown). Aligned fibers showed increased cellular alignment of the MSCs, indicated by the F-Actin stain (Figure 1D,E). Pore and fiber sizes of scaffolds were also measured via SEM (Figure 1F). While the fiber diameters remained similar in both scaffolds, larger pore sizes were observed in the random scaffolds versus aligned scaffolds (19.92 ± 7.8 vs 13.2 ± 6.5 μm). This is most likely the result of random fiber orientation leaving unequal distributions between fibers. With average cell size ranging from 10 to 30 μm,[10] our fibers provided a surface large enough for cell attachment and alignment, while pore size was concomitantly large enough to permit potential cell passage into the 3D structure of the scaffold (Figure 1F). Fiber alignment enhanced cellular attachment and promoted growth and proliferation (Figure 1, Supporting Information).

A fundamental requirement for TE scaffolds is to provide a mechanically tolerant material capable of withstanding the physiological stress and strain of a relevant tissue.[26]

Mechanical properties of random and aligned P4HB were assessed with uniaxial testing. Stress-strain curves of random and aligned scaffolds were obtained, followed by measurement of the initial stiffness through the slope of the curves (at 15% strain), at the point of failure for the Ultimate tensile strength (UTS), and at strain-to-failure (εf) (break point denoted with *) (Figure 1G,H). Stress-strain curves demonstrated different anisotropic properties between the preferred directions (PD)(aligned with fiber directions), and the cross-orthogonal direction (XD) for the aligned scaffold. This difference, however, was not observed for the randomly oriented scaffold fibers, which had similar mechanical properties in all directions (Figure 1G,H). Aligned scaffolds possessed higher UTS (2.68 ± 0.2 MPa) and lower εf (1.27 ± 0.23) in the PD direction. These studies revealed that the scaffold was stiffer in the direction of fiber alignment (PD) (stiffness $(E) = 5.68 \pm 0.75$ MPa) and more deformable in the XD direction ($\varepsilon f = 1.8 \pm 0.13$).

Moreover, the aligned arrangement of fibers improved the scaffold's mechanical properties in terms of stiffness and UTS. Anisotropy is essential to scaffold characteristics, especially in cardiac tissues, as native tissues' ECM protein fibers are aligned in specific directions.[8,12,27,28] For example, the opening of heart valve leaflets during systolic blood flow and closure during diastole depends on the elasticity and anisotropy of this tissue.[29] Myocardial stretching during the cardiac cycle also relies on tissue flexibility and anisotropy. Blood vessel elasticity modulates circulatory pressures and depends on tubular contraction and undulation, essential components that are dependent on structural anisotropy. Previous studies of other synthetic biomaterials have also shown the significance of scaffold architecture and fiber orientation in relation to biomechanics, cellular attachment, and alignment.[6,10,12,30] Thus, the anisotropic characteristic of our aligned P4HB scaffold was reasonably similar to that of some native tissues.[28,30]

Cyclic tensile tests were performed up to a maximum of 20% of the strain—which corresponds to the range of physiological deformation[31]—to evaluate the elasticity of P4HB in comparison to previous scaffolds.[6,27,32] The initial position of the scaffolds (left panel), prior to starting the subsequent 5-cycle tensile tests (right 3 panels) for each of the materials, was compared (Figure 2A). PCL scaffolds deformed considerably following the cycles due to its inherent plasticity. However, for relatively elastic materials, like PCUU, no deformation was observed following cyclic tests. Of note, no significant deformation was observed for P4HB, which suggested favorable elastic properties.

We next obtained stress-strain curves for the aforementioned cyclic tests (Figure 2B). As expected, P4HB demonstrated low energy loss (19%), which was comparable to PCUU (15%), and higher resilience to deformation compared to PCL (29%). This finding is in accordance with the linear trend of the stress-to-strain curve of P4HB, which revealed no evidence of plastic deformation when compared to the PCL stress-to-strain curve. These results were notable considering that elasticity is a property that is indispensable to the functionality of many native tissues.[4,28,33] By comparison, the energy loss of native aortic and pulmonary valve leaflets (defined as the area under the stress/strain curve, during the stretch and return of a cycle) (≈20%) is similar to that found in our P4HB scaffolds, suggesting comparable elasticity and deformability between our scaffolds and those native structures.[33] In contrast, the P4HB bulk materials have relatively low elasticity[23] and

higher stiffness (reported as tensile modulus 70 MPa and UTS 60 MPa[23]) when they are evaluated as sheets as opposed to the multiple fiber structure in our material. This difference indicates that fabrication of the P4HB as fibrous constructs resulted in more flexible and elastomeric materials.

While providing favorable structure and mechanics, synthetic scaffolds, when compared to natural hydrogels, may not be preferable, either in terms of cellular attachment or tissue ingrowth.[5] One of the concerns regarding fibrous scaffolds is variation in pore sizes (some too small and some too large),[18] which can impair cellular ingrowth within the 3D structure. If the pores are too small, cells cannot penetrate, but if the pores are too large, cells on adjacent fibers are sufficiently distant from one another to impair tissue formation. We hypothesized that filling the porous scaffold with a hydrogel, to create a hybrid structure, would overcome these problems of varying pore size on cell growth. In a sense, filling scaffolds with cel-lularized hydrogels “decouples” the need for a scaffold with defined mechanical properties from its ability to attract cells. We reasoned that introducing GelMa into the fibrous structure of P4HB would result in a hybrid P4HB/GelMa to provide not only a cell compatible environment but also one that would enhance cell growth throughout the 3D structure.

In addition to assessing this hybrid for its ability to incorporate cells, however, we tested P4HB/GelMa for its ability to hold suture and prevent fluid leakage under hydrostatic pressure. This mechanical property is a particularly important factor to consider in cardiovascular tissue engineering.[33,34] Retention tests were performed and UTS values at the point of failure were measured for bare P4HB (0.81 ± 0.15 MPa) and compared to that of the pulmonary artery (0.32 ± 0.21 MPa). Scaffolds were capable of holding sutures while maintaining shape under physiological stress equivalents (Figure 2C). Perfusion pressure tests indicated that scaffolds embedded with GelMa withstand hydrostatic pressures comparable to the results obtained from those of sheep pulmonary artery (Figure S2, Supporting Information). These results were favorable to those of bare P4HB, which demonstrated a rapid leakage of fluid through the scaffold’s fibrous structure. These mechanical properties for bare P4HB (E = 6 MPa) were also compared to the stiffness of other cardiac tissues, including aortic valve leaflet (E = 6 MPa),[30,33] ventricular myocardium (E = 0.5 MPa),[35] and aorta (E = 3 MPa).[36] The elastic modulus of P4HB, on the order of 7 MPa, which is comparable to that of the valve leaflet but these results suggest that it could also serve as a potential replacement for vascular conduits and blood vessels. (Figure 2D)

2.2. P4HB/GelMa Scaffolds Encapsulate and Maintain Cell Viability

Protein-based hydrogels have been utilized for different regenerative medicine applications because of their amino acid composition and their potential for supporting biocompatibility in in vivo environment.[37] To avoid the water solubility, these hydrogels require crosslinking reaction to stabilize the protein content within the hydrogel for in vitro or in vivo appli-cation.[16] Prior investigators have proposed using physical or chemical crosslinking processes to overcome these challenges. However, physical crosslinking while capable of rapid gelation requires unique crosslinking conditions (due to sensitivity to

temperature, PH, or ionic concentration) that would limit the use of this method for in vivo applications.[38] Chemical crosslinking, allows for the formation of permanent irreversible bonds between chemically active functional groups in the protein sequence[39] (producing crosslinks between native groups, such as amines, carboxyls, and sulfhydryls with addition of a crosslinker, for instance, glutaraldehyde). However, controlling the physical properties to tune the degradation rate is limited due to long reaction times, preventing their applications in circumstances where rapid gelation or degradation is required. Also the toxic byproducts of the chemical crosslinking techniques have been reported to be problematic.[37] Using the photo-crosslinking method in this study, we were able to form the chemical bonds within seconds and tune the physical and chemical properties of GelMA hydrogel by varying the UV radiation parameters (e.g., time and energy). Moreover, photocrosslinking technique allows for spatial and temporal control of crosslinking that facilitates the hydrogel fabrication and application.

In the past,[21] to fabricate GelMA with tunable mechanical characteristic, three different GelMA hydrogels were synthesized using 1, 5, and 10 M methacrylic anhydrate. The actual percentages of the functionalized methacrylation groups were determined by measuring the extent of free amine group substitution using 1H-NMR spectroscopy. The degree of methacryla-tion (defined as the ratio of functionalized to original amino groups) corresponded to 49.8%, 63.8%, and 73.2% for the 1, 5, and 10 M GelMA hydrogels, respectively and as expected, the compressive modulus of the GelMA increased with the degree of methacrylation. By measuring the percentage of hydrogel residual mass as a function of time, the degradation rate of the hydrogel was also determined. We found that the rate of degradation decreased with the methacrylation degree of the GelMA (1 M GelMA hydrogels were completely degraded within 6 h, whereas the 10 M GelMA hydrogels lasted for 15 h).For this study, as explained further in this section, we used the 1 M GelMA hydrogel to achieve a rapid degradation rate for our in vitro setting. In addition, we have shown that a liquid solution of GelMA injected beneath the skin can undergo polymerization rapidly (15–30 s) after this injection while continuing to support human progenitor cells and MSCs.[16]

In our study, two processes of seeding were utilized, direct surface seeding and encapsulation of cells into GelMa prior to addition to the scaffold. These two methods resulted in varied patterns of subsequent tissue formation (Figure 3A-F). The first schematic in Figure 3A shows a general 2D surface seeding of MSCs onto bare P4HB scaffolds. 7 d after seeding, histological evaluation of nuclei and quantitative analysis of cell infiltration revealed that surface seeding on bare scaffolds produced a cellularized surface but no significant cell penetration into the 3D construct or tissue growth (Figure 3B). In contrast, as shown in the second schematic, MSCs that were encapsulated in GelMa prior to exposure to the scaffold penetrated the 3D structure of the P4HB scaffold. After 7 d in the P4HB/ GelMa hybrid construct, cells not only grew along the surface of the scaffold but they also penetrated into the 3D structure of the scaffold (Figure 3E). Both methods of seeding (2D and 3D) retained cell viability, as demonstrated by Live/Dead assays (Figure 3C,F, respectively).

Cellular encapsulation with hydrogels, to create a 3D-tissue environment, has previously been reported as a technique in tissue engineering.[40] However, for load bearing tissues, soft hydrogels alone do not satisfy the mechanical strength and anisotropic requirements of relevant tissues. We showed that successfully integrating cells into fibrous P4HB with GelMa resulted in a 3D cell seeding without significantly affecting the mechanical properties of the scaffold. Of note, the requirements of both synthetic materials and hydrogels were decoupled with our combination of P4HB/GelMa. On the one hand, fibrous scaffolds often present an environment that is difficult for cells to penetrate in a 3D manner; on the other hand hydrogels do not provide sufficient mechanical strength for certain tissue engineering applications. In this regard, P4HB/GelMa is a novel material that combines the properties of a mechanically favorable, fibrous scaffold with those of a hydrogel that can encapsulate cells for growth within a 3D environment.

2.3. Structural Microscopy Confirms Retention of Cells in P4HB/GelMa Scaffolds

We compared the structure of bare P4HB and P4HB/GelMa at 1 d of culture using SEM (Figure 3G,H). Scaffolds with GelMa showed a smoother surface structure as the gel permeated the scaffold pores and created a homogenous layer of GelMa on the surface and throughout the fibers (Figure 3H). A series of experiments were performed to obtain the optimum GelMa stiffness to optimize spreading and attachment of cells during cultivation. Results confirmed that an increase in the degree of crosslinking of GelMa, obtained by longer UV exposure or higher UV intensity, impaired cell spreading. Similar results were reported in a recent study of encapsulated valvular interstitial cells in GelMa.[19] Moreover, a large number of the cells did not remain attached to the scaffolds after mechanical stimulation, which could have resulted from the connection of the cells to the hydrogel instead of P4HB. To overcome this limitation and preserve cell and tissue formation throughout the scaffold, we optimized the degree of crosslinking for GelMa to provide the scaffolds with a specific stiffness. At our point of optimization, GelMa formed and encapsulated the cells within the scaffold's 3D structure, but the GelMa then degraded during a one-week static culture. This degree of crosslinking also allowed cells to attach to P4HB scaffold's fibers and spread throughout the interior layers of the scaffold compared to penetration with increasingly solid GelMa structures (qualitative data to explain degree of crosslinking shown in Figure 3, Supporting Information).

Following 7 d of culture, the scaffolds from each of the seeded conditions were fixed for SEM imaging (Figure 3I-K). When GelMa, without cells, was added to scaffolds, GelMa disappeared almost completely after 7 d and the underlying fiber structure was visualized (Figure 3I). When P4HB was seeded with both GelMa and cells, tissue formation appeared and was distributed more evenly (compared to when P4HB was seeded with MSCs directly on the surface) as GelMa disappeared over the 7 d timeline (Figure 3J,K). Following 7 d, the similarity between the structure of the bare P4HB scaffolds and P4HB/GelMa without cells suggested that GelMa had degraded after 7 d of incubation (Figure 3G,I). Additionally, the proliferation of cells and concomitant disappearance of GelMa (in Figure 3J) was confirmed when compared to the empty pores of P4HB/GelMa without cells (in Figure 3I). These results suggested that GelMa played a role in enhancing cell penetration into the 3D structure of P4HB but degraded after 7 d and thus did not prevent cell growth and

proliferation as shown by the DNA assay, quantifying cell number, explained in following section.

2.4. Cell-Seeded P4HB/GelMa Scaffolds Affect Mechanical Properties and Tissue Formation in in Vitro Bioreactor Conditions More than in Static Culture

Following examination of mechanical properties and integration of cells throughout the 3D structure of the scaffolds, P4HB/GelMa was tested in a stretch/flex bioreactor that we previously designed and tested for growing fibroblast and valvular interestitial cells.[24] The scaffold's deformation and tissue formation were then assessed after exposure to physiological stresses and flexure. Schematic, design, and functional portraits of the stretch-flex bioreactor used in this study are depicted, respectively, in Figure 4A-D. More specifically, Figure 4C,D show P4HB/GelMa scaffolds in the flex (C) and stretch configurations (D). The detail of the scaffolds' culture in the bioreactor can be found in the Supporting Information. Scaffolds were seeded and cultured statically (7 d) prior to implanting them in the bioreactor, for another 7 d. Samples were stretched and flexed initially with a lower strain rate (1 cycle 3.5 s^{-1}) compared to physiological rates (1 cycle 1.3 s^{-1}) to allow the cells to acclimate to the imposed mechanical stress environment. This accommodation protocol prevented loss of cells during the initial time of cultivation in the bioreactor, which had been seen in pilot experiments where samples were initially stretched and bent with a higher strain rate (data not shown).

To evaluate the effect of 15% stretch and 20% flexure (based on radius of curvature as we previously described in the design of the bioreactort[19]) on tissue formation on the scaffolds, samples were assessed with biochemical assays (i.e., DNA and collagen content) and compared to the statically cultured samples. Variations in DNA and collagen content between static scaffolds and those stretched and flexed in the bioreactor are denoted in Figure 4E-G. Results confirmed that the static condition produced more DNA (14.35 ± 3.09 vs 4.29 ± 2.41 μg g^{-1} wet weight), but the amount of collagen produced was not statistically different compared to that of the bioreactor condition (2.06 ± 0.92 vs 1.72 ± 0.64 μg g^{-1} wet weight). The average value of DNA obtained from the bioreactor condition was comparable to the DNA obtained from the samples that were cultured in a static condition for 7 d, prior to bioreactor implantation (average of 4.5 μg g^{-1} wet weight). This finding indicates that DNA did not increase significantly in the bioreactor condition versus the static condition. Therefore, the lower amount of DNA in samples from the bioreactor was likely due to the enzymatic activities of the cells that produced ECM production rather than cell proliferation. Also, the ratio of total micrograms of collagen produced per microgram of DNA, which was higher in the bioreactor samples than the static samples, supports the aforementioned conclusion (Figure 4G), and is consistent with previous studies.[24,41] Thus, fewer cells, which correlate to the lower amount of DNA, produced a larger total mass of collagen rather than an increased number of cells (and DNA) being responsible for increased collagen levels. Similar results were obtained when random P4HB scaffolds were seeded with a higher density of MSCs. The finding that cell seeding onto aligned fiber scaffolds resulted in increased stiffness and UTS (E = 5.66 ± 1.24 MPa and UTS = 2.22 ± 0.53 MPa) and deformation (εf = 5.92 ± 0.96) compared to unseeded aligned fiber scaffolds seems likely to be the result of tissue production in the cell-seeded scaffolds (Figure 4). This finding was

present in both static and dynamic culture environments. The trend was similar for the effect of cell seeding on random fiber scaffolds (Figure 4, Supporting Information).

F-actin staining was used to evaluate the presence and adequate spreading of MSCs on P4HB after one week of static seeding, followed by 7 d cultivation in the stretch/flex bioreactor (Figure 4H). Mechanical properties were assessed following 14 d static culture to evaluate the effect of tissue formation on the mechanical properties of the P4HB scaffolds. Data was compared with initial and control (non-seeded) mechanical properties (Figure 4I). The initial stiffness of the cell-seeded P4HB-GelMA scaffolds (5.68 ± .75 MPa) and UTS (2.68 ± 0.2 MPa) was greater than uncellularized conditions following a two-week culture (E = 4.81 ± 1.19 MPa and UTS = 1.88 ± 0.34 MPa), which indicated a degradation of the scaffolds during the culture period. However, the improved mechanical properties (E = 5.66 ± 1.24 MPa and UTS = 2.22 ± 0.53 MPa) and deformation (εf= 5.92 ± 0.96) of seeded scaffolds versus unseeded scaffolds and initial condition confirmed the presence of tissue formation and ECM production (see Figure S5 in the Supporting Information for similar results of random scaffolds cultured in static condition. We hypothesize that the reduction in stiffness and UTS which are observed in both seeded and unseeded random fiber scaffolds represent surface hydrolysis of the P4HB fibers. This finding is offset to some degree (not statistically significant) by the presence of cells on the random fibers as in Figure S5 in the Supporting Information).

Biomechanical tests, for both seeded and unseeded conditions, were repeated for bioreactor samples and compared with static conditions (Figure 4J-L). The stiffness for unseeded samples increased in the bioreactor (6.58 ± 1 MPa), suggesting an induced alignment of fibers as the fibers were stretched with a resulting change in overall stiffness (Figure 4J). Similar results were found when random fibers were implanted in the bioreactor (Figure 4, Supporting Information). Higher values of stiffness for seeded samples (6.99 ± 0.87 MPa) in the bioreactor, versus static conditions, seemed to correspond with higher collagen/DNA values.

The UTS for the bioreactor samples with cells remained unchanged when compared with the static scaffold data (2.33 ± 0.19 MPa). The bioreactor samples without cells, in contrast, showed a slight decrease in UTS (1.48 ± 0.33 MPa) when compared to the unseeded static samples (Figure 4K). Analogous to the UTS data, bioreactor samples with cells showed similar deformation when compared with statically seeded scaffolds in strain-to-failure measurements (0.75 ± 0.12 MPa vs 0.67 ± 0.14 MPa). Bioreactor samples without cells, however, showed decreased strain-to-failure properties compared to static samples, as well as seeded bioreactor samples; this could be related to faster degradation of the scaffolds under mechanical stimulation (Figure 4L). These results suggest that, when exposed to stretch and flexing, cell seeded scaffolds show greater resistance to deformation and can withstand greater strain than those without cells under the same conditions. This data suggested that cellular seeding could support the mechanical properties of scaffolds in both static and bioreactor conditions.

2.5. P4HB/GelMa Remains Functional Under Physiological Stress In Vivo

To evaluate the biocompatibility and functionality of the novel hybrid scaffold, we implanted P4HB/GelMa as a pulmonary artery patch in a sheep model previously described by our group (see Surgical Implantation, Supporting Information; Figure 5A). Figure 5B,C depicts the scaffolds—both sutured to the pulmonary artery and explanted—7 d post implantation. Autologous ovine MSCs and endothelial progenitor cells (EPCs) were used to seed the hybrid scaffold statically for 6 d prior to implantation. We previously conducted a thrombogenicity assay and determined that seeding the hybrid scaffold with autologous EPCs prevented thrombus formation (Figure 6, Supporting Information). In vivo, coating both surfaces of the hybrid scaffold with autologous EPCs also reduced the formation of surface thrombi (Figure 5C-E). The explanted samples were cut and prepared for hematoxylin and eosin (H&E) staining on cross-sectional (D) and surface-oriented (E) cuts (Figure 5D,E). H&E-stained sections showed tissue formation and cellularity throughout the scaffold. In addition, there was noticeable alignment of tissue matrix formed within the scaffold. Of note, this alignment occurred in the direction of blood flow (indicated by dark pink staining on Figure 5D). Finally, the presence of myofibroblasts was confirmed by alpha-smooth muscle actin (α-SMA) staining (Figure 5F,G). Myofibroblasts were seen abundantly within the center of the scaffolds, which indicated penetration and retention of cells. Collectively, this in vivo evaluation confirmed that our cell-seeded hybrid scaffold were non-thrombogenic and were capable of withstanding physiological pressures in the pulmonary artery.

3. Conclusion

In summary, we introduce a platform to develop a biocompatible hybrid fibrous scaffold, derived from a synthetic polymer and a natural hydrogel that facilitated cell attachment, ingrowth and elongation along the fiber direction. Our initial target was to match the constructs' mechanical properties and structure with the native tissue's properties, such as ECM composition and organization, as well as mechanical stiffness and anisotropy. In attempt to mimic native tissues compositions and overcome the challenge of cell ingrowth in fibrous constructs, we used photo-crosslinkable GelMA to encapsulate cells, an approach that resulted in 3D tissue formation throughout the hybrid scaffold. Photodegradable GelMA was shown to be sensitive to UV irradiation; enabling us to manipulate the physical properties and degradation rate of the hydrogel within the scaffolds. Combining the two materials offered a cell compatible environment while providing sufficient mechanical support and structural anisotropy. Our hybrid scaffolds were able to guide the cellular arrangement due to their fiber orientation by providing a dynamic cell culture substrate due to the presence of photodegradable GelMA hydrogels, which resembled native tissue architectures. Our results suggest that the hybrid scaffold may serve as a suitable replacement to address the requirements for cardiovascular tissue engineering. Furthermore, our in vivo evaluations revealed excellent biocompatibility and minimal degradation, resulting in early and progressive ingrowth of host tissue for the hybrid scaffolds, confirming that the material is 1) capable of withstanding physiological pressures on the surface of the pulmonary artery, 2) does not induce clot formation, 3) permits myofibroblast activity across the scaffold, and 4) produces aligned tissue growth on the scaffold surface that is in contact

with blood. Additional studies are currently underway to further identify potential applications for this novel hybrid material within the field of cardiovascular tissue engineering.

4. Experimental Section

P4HB (M_w = 390 kDa, Tepha, Inc. Lexington, MA) was biosynthesized using a recombinant strain of *Escherichia coli* K12 and was isolated and purified as previously described.[23] The chemical structure of P4HB is shown in Figure 1A. Highly porous nonwoven scaffolds of P4HB were prepared with a novel dry spinning technique. In brief, P4HB was dissolved in chloroform (8% (w/v)) to create a viscous solution that was sprayed through an automatic spraying gun (Model RA 5, Krautzberger GmbH, Germany) using compressed air to draw and attenuate the fibers as they departed the spray nozzle. The solvent evaporated during the flight of the polymer strands to create continuous micrometer-sized fibers of consistent diameter (≈1.8 μm). The fibers were collected on a flat fiberglass filter at a working distance of 33” from the spray nozzle to obtain the random nonwoven scaffolds. P4HB nonwoven scaffolds with highly aligned fibers and anisotropic properties were prepared by using a rotating mandrel collector (OD: 3.25”, working distance: 27”) with a rotational speed of 1166 rpm as shown in Figure 1A.

GelMa was synthesized as described previously from type-A porcine skin gelatin (Sigma-Aldrich).[14] The methacrylation process, under stirring conditions, is described in detail in the Supporting Information. The GelMa solution was dialyzed against deionized (DI) water, stored frozen at −80 °C, lyophilized, and again stored in the freezer. Before use for cell seeding processes, a GelMa prepolymer solution was prepared by dissolving the freeze-dried GelMa (5% (w/v) final) and the photo initiator (Irgacure 2959) (0.5% (w/v), CIBA Chemicals) in Dulbecco’s phosphate buffered saline (DPBS) at 60 °C. Photo-crosslinking was achieved by exposing the GelMa prepolymer to 6.7 mW cm^{-2} UV light (360–480 nm; using an OmniCure S2000 UV lamp (Lumen Dynamics)) for 20 s at room temperature.

The scaffolds were tested with a uniaxial mechanical tester (Instron 5542) to assess the mechanical characteristics of the unseeded scaffolds initially and after a four-week culture period (soaked in medium). The samples were then sterilely prepared for cell seeding and soaked in media for 2 d. The detailed MSC and EPC isolation has been described in the Supporting Information. The animal protocol was approved by the Institutional Animal Care and Use Committee at Boston Children’s Hospital (protocol #13–10-2531R). Bone marrow samples were obtained from sheep femurs in Animal Research Children’s Hospital (ARCH, Boston). For EPC isolation blood was derived from sheep donor. The blood was aspirated into a heparinized syringe (20–40 mL blood drawn from the right femoral vein using 19-guage needle). The MSCs were seeded directly on the scaffolds or were suspended (1×10^6 cm^{-2} of the scaffold in 80 μL) in the GelMa solution (500 mg GelMa, 10 mL PBS with 5% photo initiator dissolved in the PBS). Photo-crosslinking was achieved by exposing the cell-prepolymer mixture to UV light (360–480 nm) for 15 s. Thereafter, cell-laden hydrogels encapsulated in fibrous scaffolds were cultured in Dulbecco’s Modified Eagle Medium (DMEM) for a week in static culture. Following a one-week static seeding, eight scaffolds (prepared as described in the Supporting Information) were placed in the bioreactor for

further culturing in flexure and stretch condition. For comparison, eight more samples were retained for continued study in the static conditions. At the end of the culture time, samples were cut and prepared for the biochemical assays, including collagen and DNA assays, to assess the tissue formation and cellular proliferation. Samples were also fixed and cut for histology and immunohistochemistry (details can be found in the Supporting Information).

Supplementary Material

Refer to Web version on PubMed Central for supplementary material.

References

[1]. Brody S, Pandit A, J. Biomed. Mater. Res., Part B 2007, 83, 16.

[2]. Vacanti JP, Langer R, Lancet 1999, 354, S32.

[3]. Hutmacher DW, Biomaterials 2000, 21, 2529. [PubMed: 11071603]

[4]. Sacks MS, Schoen FJ, Mayer JE, Annu. Rev. Biomed. Eng. 2009, 11, 289. [PubMed: 19413511]

[5]. Annabi N, Mithieux SM, Zorlutuna P, Camci-Unal G, Weiss AS, Khademhosseini A, Biomaterials 2013, 34, 5496. [PubMed: 23639533]

[6]. Masoumi N, Annabi N, Assmann A, Larson BL, Hjortnaes J, Alemdar N, Kharaziha M, Manning KB, Mayer JE, Khademhosseini A, Biomaterials 2014, 35, 7774. [PubMed: 24947233]

[7]. Rouwkema J, Rivron NC, van Blitterswijk CA, Trends Biotechnol.2008, 26, 434. [PubMed: 18585808]

[8]. Masoumi N, Larson BL, Annabi N, Kharaziha M, Zamanian B, Shapero KS, Cubberley AT, Camci-Unal G, Manning K, Mayer JE, Adv. Healthcare Mater. 2014, 3, 929.

[9]. Masoumi N, Jean A, Zugates JT, Johnson KL, Engelmayr GC Jr., J. Biomed. Mater. Res. Part A 2013, 101, 104.

[10]. Kolewe ME, Park H, Gray C, Ye X, Langer R, Freed LE, Adv Mater. 2013, 25, 4459. [PubMed: 23765688]

[11]. Gottlieb D, Kunal T, Emani S, Aikawa E, Brown DW, Powell AJ, Nedder A, Engelmayr GC Jr., Melero-Martin JM, Sacks MS, Mayer JE Jr.,J. Thorac. Cardiovasc. Surg. 2010, 139, 723. [PubMed: 20176213]

[12]. Kharaziha M, Nikkhah M, Shin SR, Annabi N, Masoumi N, Gaharwar AK, Camci-Unal G, Khademhosseini A, Biomaterials 2013, 34, 6355. [PubMed: 23747008]

[13]. Niu H, Mu J, Zhang J, Hu P, Bo P, Wang Y,J. Mater. Sci.: Mater. Med. 2013, 24, 1535. [PubMed: 23620011]

[14]. Hashizume R, Hong Y, Takanari K, Fujimoto KL, Tobita K, Wagner WR, Biomaterials 2013, 34, 7353. [PubMed: 23827185]

[15]. Drury JL, Mooney DJ, Biomaterials 2003, 24, 4337. [PubMed: 12922147]

[16]. Lin R-Z, Chen Y-C, Moreno-Luna R, Khademhosseini A, Melero-Martin JM, Biomaterials 2013, 34, 6785. [PubMed: 23773819]

[17]. Robinson PS, Johnson SL, Evans MC, Barocas VH, Tranquillo RT, Tissue Eng. Part A 2008, 14, 83. [PubMed: 18333807]

[18]. Baker BM, Gee AO, Metter RB, Nathan AS, Marklein RA, Burdick JA, Mauck RL, Biomaterials. 2008, 29, 2348. [PubMed: 18313138]

[19]. Eslami M, Vrana NE, Zorlutuna P, Sant S, Jung S, Masoumi N, Khavari-Nejad RA, Javadi G, Khademhosseini A, J. Biomater. Appl. 2014, 29, 399. [PubMed: 24733776]

[20]. Rice JJ, Martino MM, De Laporte L, Tortelli F, Briquez PS, Hubbell JA, Adv. Healthcare Mater. 2013, 2, 57.

[21]. Chen YC, Lin RZ, Qi H, Yang Y, Bae H, Melero-Martin JM, Khademhosseini A, Adv Funct. Mater. 2012, 22, 2027. [PubMed: 22907987]

[22]. a) Duan B, Hockaday LA, Kang KH, Butcher JT, J. Biomed. Mater. Res., Part A 2013, 101, 1255;b) Hjortnaes J, Camci-Unal G, Hutcheson JD, Jung SM, Schoen FJ, Kluin J, Aikawa E, Khademhosseini A, Adv Healthcare Mater. 2015, 4, 121.

[23]. Martin DP, Williams SF, Biochem. Eng. J. 2003, 16, 97.

[24]. Masoumi N, Howell MC, Johnson KL, Niesslein MJ, Gerber G, Engelmayr GC Jr., Proc. Inst. Mech. Eng., Part H 2014, 228, 576.

[25]. a) Sierad LN, Simionescu A, Albers C, Chen J, Maivelett J, Tedder ME, Liao J, Simionescu DT, Cardiovasc. Eng. Technol. 2010, 1, 138; [PubMed: 21340043] b) Tranquillo RT, Ann. N. Y. Acad. Sci. 2002, 961, 251; [PubMed: 12081910] c) Kim BS, Nikolovski J, Bonadio J, Mooney DJ, Nat. Biotechnol. 1999, 17, 979. [PubMed: 10504698]

[26]. a) Sacks MS, David Merryman W, Schmidt DE, J. Biomech. 2009, 42, 1804; [PubMed: 19540499] b) Frank BS, Toth PB, Wells WK, McFall CR, Cromwell ML, Hilbert SL, Lofland GK, Hopkins RA,J. Surg. Res. 2012, 174, 39. [PubMed: 21345451]

[27]. Courtney T, Sacks MS, Stankus J, Guan J, Wagner WR, Biomaterials 2006, 27, 3631. [PubMed: 16545867]

[28]. Engelmayr GC, Cheng M, Bettinger CJ, Borenstein JT, Langer R, Freed LE, Nat. Mater. 2008, 7, 1003. [PubMed: 18978786]

[29]. Sacks MS, Yoganathan AP, Philos. Trans. R. Soc., B 2007, 362, 1369.

[30]. Masoumi N, Johnson KL, Howell MC, Engelmayr GC Jr., Acta Biomater. 2013, 9, 5974. [PubMed: 23295404]

[31]. Stella JA, Liao J, Hong Y, Merryman WD, Wagner WR, Sacks MS, Biomaterials 2008, 29, 3228. [PubMed: 18472154]

[32]. Hong Y, Guan J, Fujimoto KL, Hashizume R, Pelinescu AL, Wagner WR, Biomaterials 2010, 31, 4249. [PubMed: 20188411]

[33]. Masoumi N, Annabi N, Assmann A, Larson BL, Hjortnaes J, Alemdar N, Kharaziha M, Manning KB, Mayer JE Jr., Khademhosseini A, Biomaterials 2014, 35, 7774. [PubMed: 24947233]

[34]. Tran RT, Thevenot P, Zhang Y, Gyawali D, Tang L, Yang J, Materials 2010, 3, 1375. [PubMed: 21113339]

[35]. Sommer G, Schwarz M, Kutschera M, Kresnik R, Regitnig P, Schriefl A, Wolinski H, Kohlwein S, Holzapfel GA, Biomed. Eng./ Biomed. Tech. 2013, 58 (Suppl. 1), 4108.

[36]. Duprey A, Khanafer K, Schlicht M, Avril S, Williams D, Berguer R, Eur. J. Vasc. Endovasc. Surg. 2010, 39, 700. [PubMed: 20346708]

[37]. MacEwan SR, Chilkoti A, Pept. Sci. 2010, 94, 60.

[38]. Zhang YN, Avery RK, Vallmajo-Martin Q, Assmann A, Vegh A, Memic A, Olsen BD, Annabi N, Khademhosseini A, Adv. Funct. Mater. 2015, 25, 4814. [PubMed: 26523134]

[39]. a) Raphel J, Parisi-Amon A, Heilshorn SC,J. Mater. Chem. 2012, 22, 19429; [PubMed: 23015764] b) Chou C, Uprety R, Davis L, Chin JW, Deiters A, Chem. Sci. 2011, 2, 480.

[40]. Benton JA, DeForest CA, Vivekanandan V, Anseth KS, Tissue Eng. Part A 2009, 15, 3221. [PubMed: 19374488]

[41]. Engelmayr GC Jr., Soletti L, Vigmostad SC, Budilarto SG, Federspiel WJ, Chandran KB, Vorp DA, Sacks MS, Ann. Biomed. Eng. 2008, 36, 700. [PubMed: 18253834]

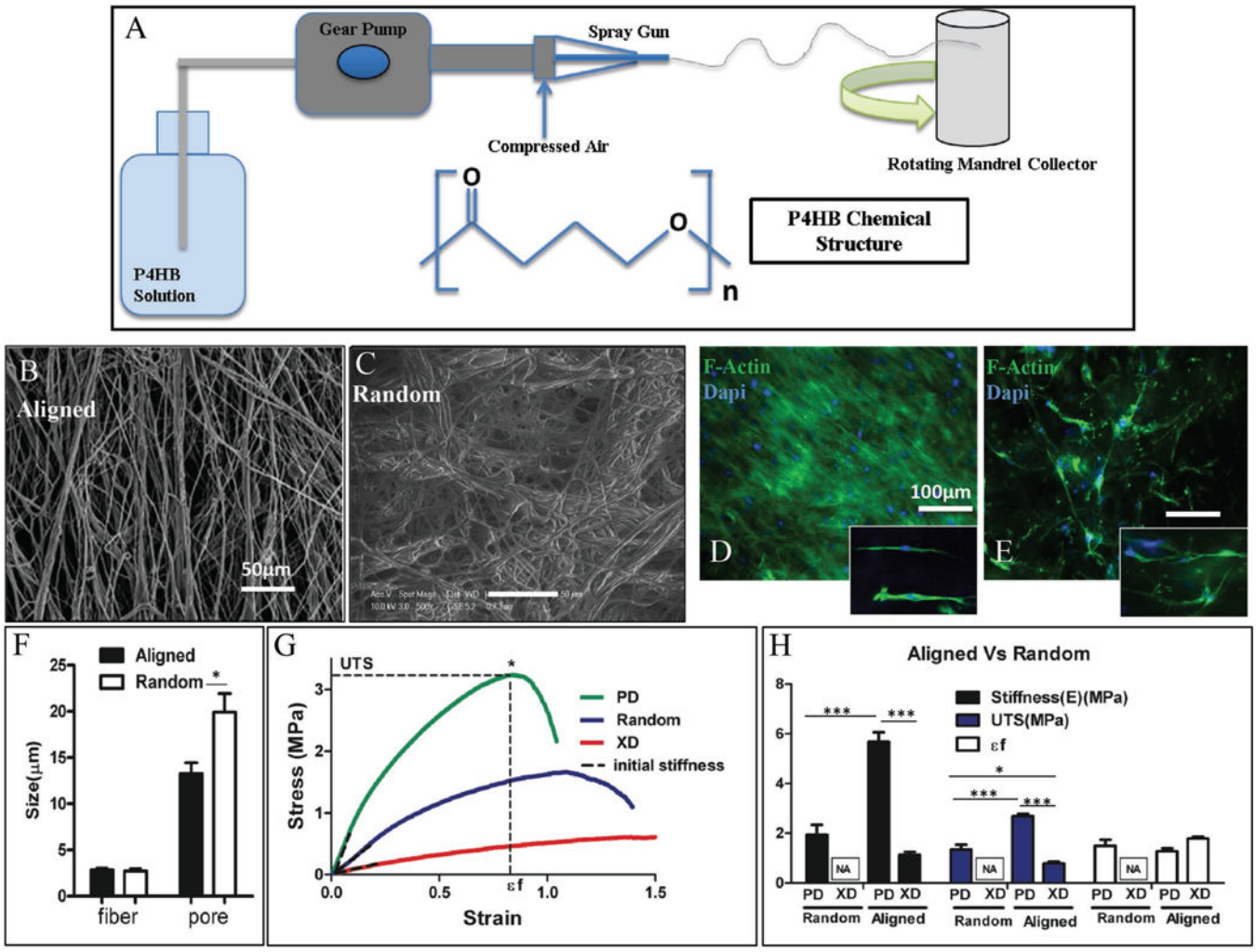

Figure 1.

Physical production and mechanics of P4HB. A) Schematic and chemical structure of novel, dry spun P4HB material. SEM images of B) aligned and C) random P4HB fibers to show variation in fiber arrangement. D,E) F-actin images comparing cellular alignment and spreading on aligned and random fibers of P4HB scaffolds. Aligned fibers show an increased number of cellular connections due to organized arrangement of cells in the fiber direction. F) Comparison of fiber and pore sizes for aligned and random fibers within sheets of P4HB. While the fiber sizes remain relatively similar in both types, the pore sizes in aligned sheets are smaller than those of the random sheets, which suggests that it can promote cellular connectivity and communication. The results correspond with the SEM images. G) Representative of the stress-strain curve for the aligned and random scaffolds confirms the anisotropic mechanical properties of the scaffolds containing aligned fibers. H) Comparison of the mechanical characteristics of both random and aligned fiber sheets of P4HB.

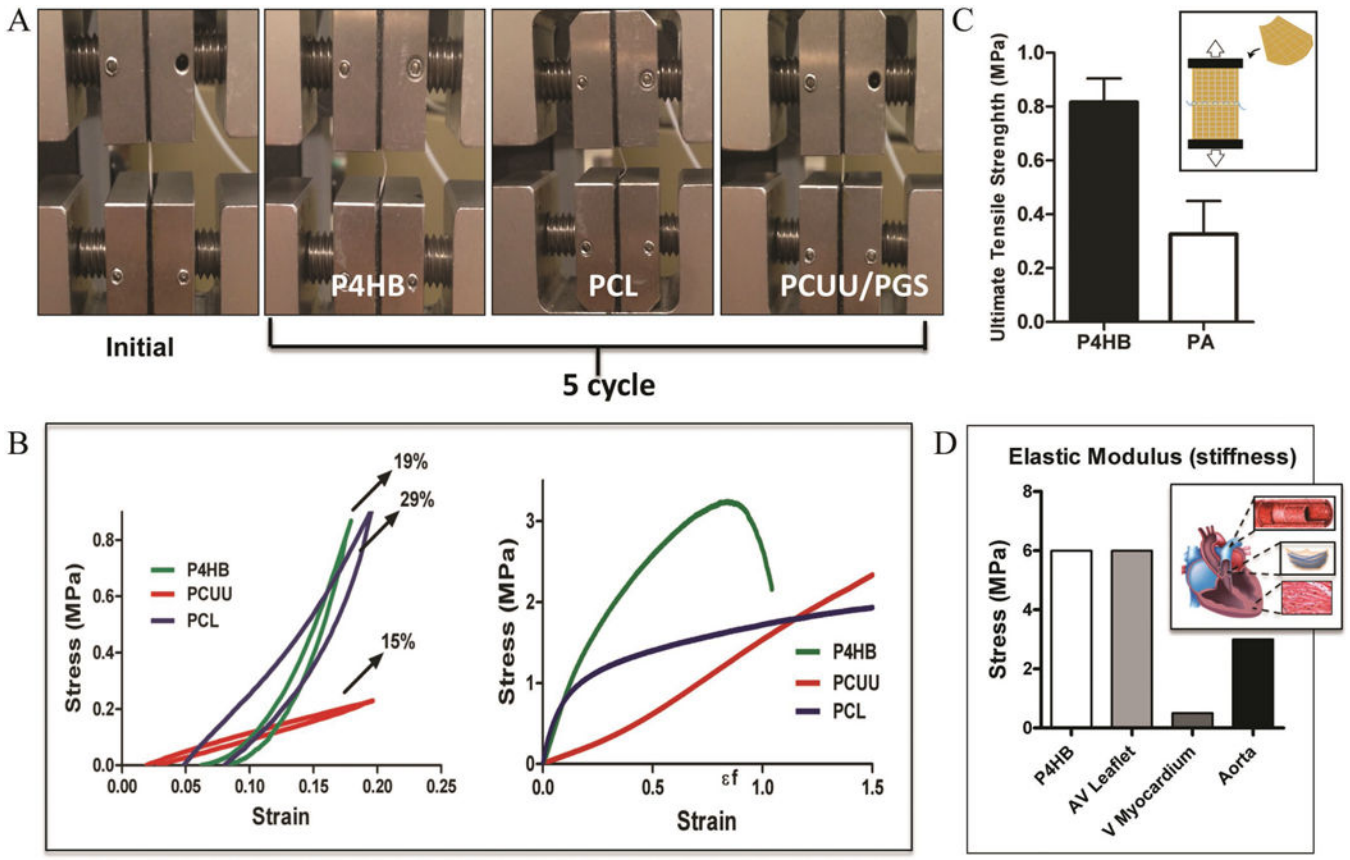

Figure 2.

Cyclic tensile tests among various scaffold materials. A) Image on far left panel represents the initial position of scaffolds before cyclic tests where the scaffold positioned is held straight between the gauges. The subsequent images represent the deformed position of each material following five cycles. B) Representative of the stress-strain curves for each of the fibrous scaffolds (P4HB, PCL, PCUU/PGS). Similar to elastic PCUU, P4HB showed little-deformation. C) When sutured, P4HB retained sutures and withstood ultimate tensile stresses to a higher degree than that of sheep pulmonary artery. D) The elastic modulus of P4HB proved to be comparable to many other cardiac tissues and was most similar to valve leaflets and aortic vessels.

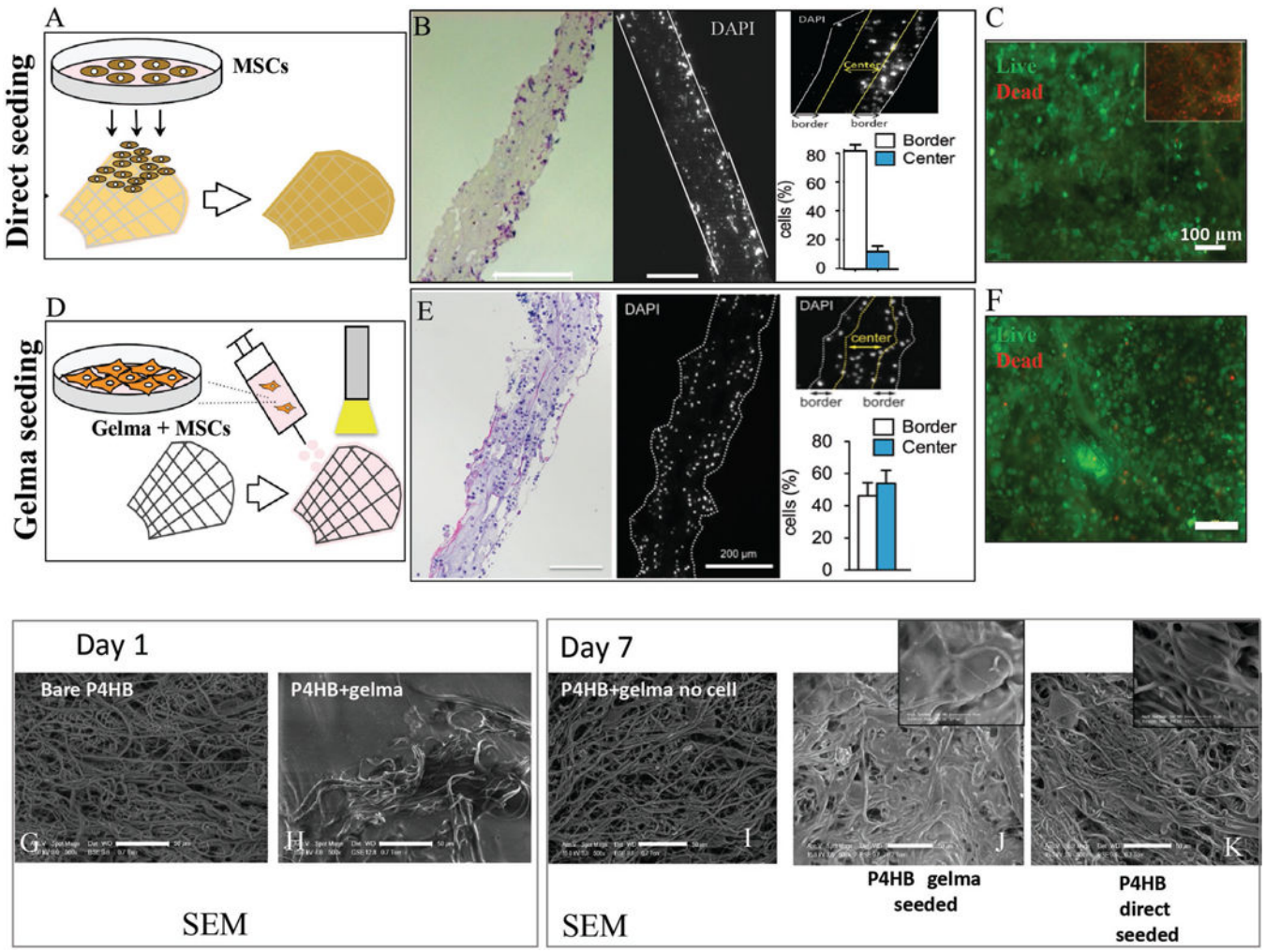

Figure 3.

Cellular encapsulation, distribution and viability were examined prior to implantation. A) Schematic of MSC direct surface seeding onto bare P4HB. B) Histology showing the cellular distribution on scaffolds. For direct surface seeding, the cells did not penetrate the scaffold and remained primarily attached to the surface layer. C) Live/Dead assay confirmed the viability of cells on those scaffolds. D-F) Schematic of the cell encapsulation with GelMa on P4HB. Histology and DAPI analysis confirmed that the cell distribution here is seen throughout the scaffold. SEM images compare the pore and surface variations at day 1 between G) bare P4HB and H) hybrid P4HB/GelMa. The pores are completely filled with crosslinked GelMa compared with the bare P4HB scaffold. SEM images from day 7 show the pore and surface variations for scaffolds: hybrid with no cells I), hybrid with encapsulated MSCs J), and bare P4HB with direct surface seeding K). J) shows cells spread more evenly and some tissue formation, especially when compared to I) in which GelMa degraded and left an uneven, porous surface.

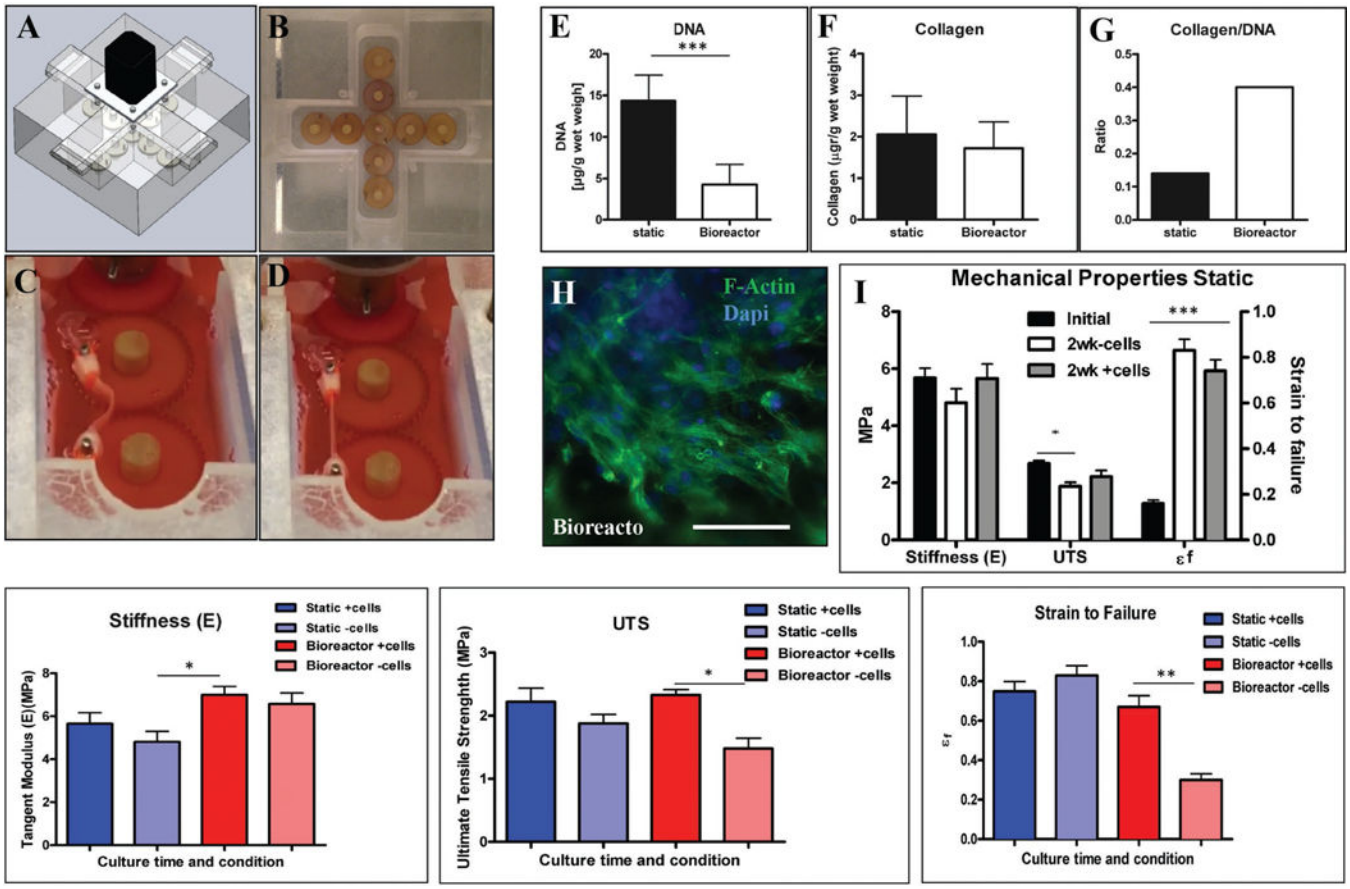

Figure 4.

Mechanical properties of hybrid scaffolds with MSCs were compared in both static and bioreactor conditions. A,B) Schematic representation and actual images of the stretch-flex bioreactor used. Image of the scaffold in flexed C) and stretch D) states within the bioreactor. E-G) Comparison of collagen, DNA, and collagen/DNA values determined from both static and bioreactor cultures. Though DNA values were higher in the static samples, the collagen produced per DNA was higher in the bioreactor, suggesting that physical stimulation increased cellular enzymatic activity. H) F-actin confirms the presence and progression of MSCs across the scaffold following bioreactor cultivation. Comparison of hybrid scaffold mechanical properties in both I) static and J-L) bioreactor conditions, with and without cells over the two-week culture time. The presence of cells increased the some mechanical values in hybrid scaffolds placed in both static and bioreactor conditions. Higher stiffness for scaffolds without cells in the bioreactor suggests increased alignment but lower UTS, and higher deformation for these scaffolds is due to the higher rate of degradation under mechanical stimulation. The increased values of stiffness and UTS for the scaffolds with the cells confirmed that scaffolds hold their integrity and ECM generation, which correlated with collagen/DNA data results in improved mechanical properties.

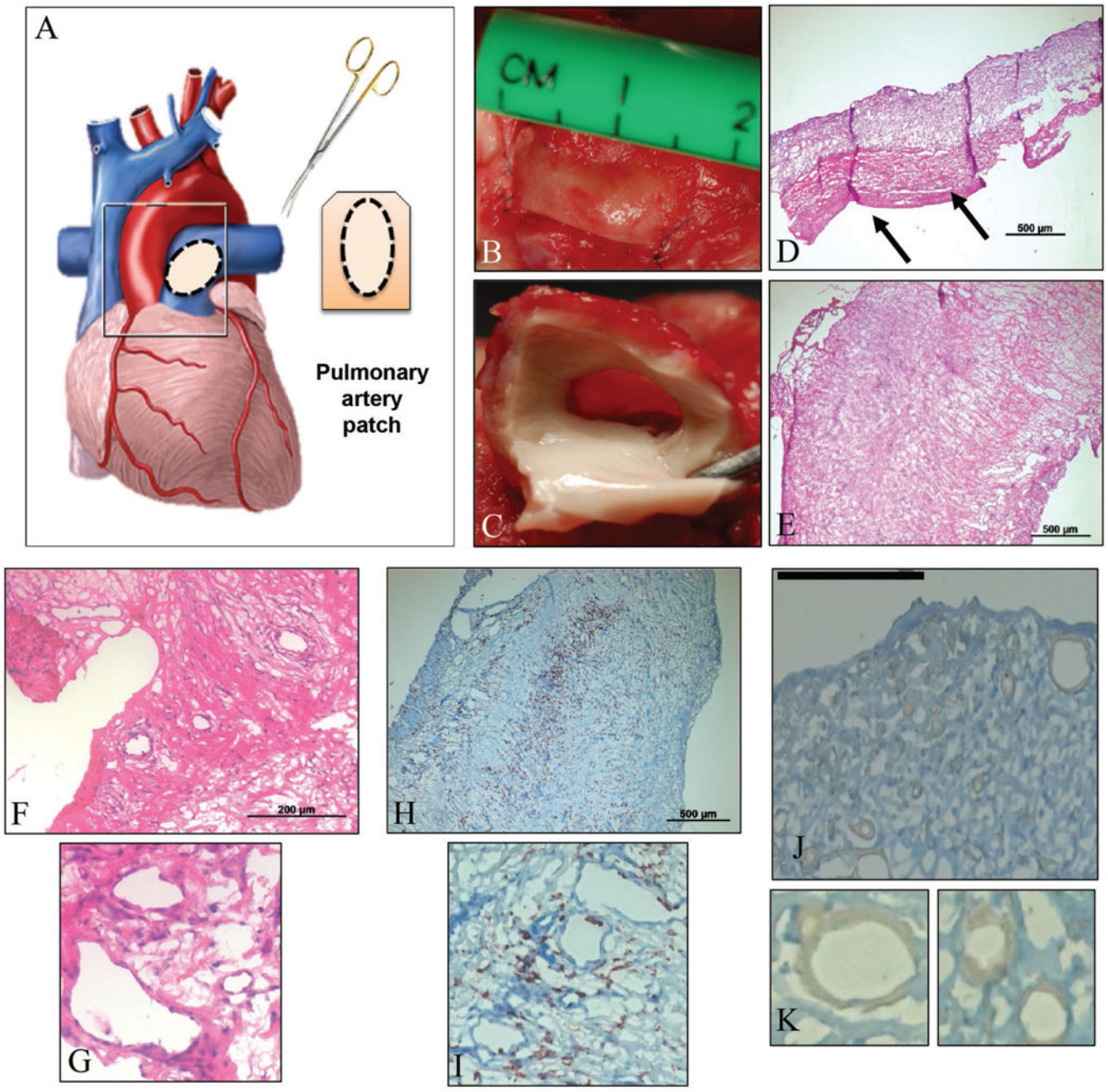

Figure 5.

In vivo experiments assessed the functionality of hybrid scaffolds under physiological pressure and stress. A) Schematic of the hybrid patch sized, cut, and placed as a patch on sheep pulmonary artery. Actual images from surgical patch implant, both with sutures, prior to explant B) and post-explant of patch with native tissue attached C). Images D) and E) portray standard H&E stains of the hybrid scaffold with tissue formation, post-explant, in cross-sectional D) and surface E) orientations. F,G) Magnifications of the H&E stains show presence of cells and sites of potential lumen formation. H,I) Hybrid scaffolds were also stained for α-SMA to confirm cell integrity and motility. The majority of cells were within

the interior of the scaffold. J,K) Stains for CD45 were performed to confirm the presence of various cell types, if any, but the stain was inconclusive; magnifications K) suggest possible sites where cells are beginning to line preliminary lumen.